

## In-situ DRIFTS and NAP-XPS Exploration of the Complexity of CO<sub>2</sub> Hydrogenation over Size Controlled Pt Nanoparticles Supported on Mesoporous NiO

András Sápi, Gyula Halasi, Janos Kiss, Dorina G. Dobó, Koppány L. Juhász, Vanessza J Kolcsár, Zsuzsa Ferencz, Gabor Vari, Vladimír Matolín, András Erd#helyi, Akos Kukovecz, and Zoltán Kónya

*J. Phys. Chem. C*, **Just Accepted Manuscript** • DOI: 10.1021/acs.jpcc.8b00061 • Publication Date (Web): 21 Feb 2018

Downloaded from <http://pubs.acs.org> on February 24, 2018

### Just Accepted

“Just Accepted” manuscripts have been peer-reviewed and accepted for publication. They are posted online prior to technical editing, formatting for publication and author proofing. The American Chemical Society provides “Just Accepted” as a service to the research community to expedite the dissemination of scientific material as soon as possible after acceptance. “Just Accepted” manuscripts appear in full in PDF format accompanied by an HTML abstract. “Just Accepted” manuscripts have been fully peer reviewed, but should not be considered the official version of record. They are citable by the Digital Object Identifier (DOI®). “Just Accepted” is an optional service offered to authors. Therefore, the “Just Accepted” Web site may not include all articles that will be published in the journal. After a manuscript is technically edited and formatted, it will be removed from the “Just Accepted” Web site and published as an ASAP article. Note that technical editing may introduce minor changes to the manuscript text and/or graphics which could affect content, and all legal disclaimers and ethical guidelines that apply to the journal pertain. ACS cannot be held responsible for errors or consequences arising from the use of information contained in these “Just Accepted” manuscripts.



# In-situ DRIFTS and NAP-XPS Exploration of the Complexity of CO<sub>2</sub> Hydrogenation over Size Controlled Pt Nanoparticles Supported on Mesoporous NiO

*András Sápi<sup>\*,†,‡</sup>, Gyula Halasi<sup>†,‡</sup>, János Kiss<sup>ψ,‡</sup>, Dorina G. Dobó<sup>†</sup>, Koppány L. Juhász<sup>†</sup>,  
Vanessza J. Kolcsár<sup>†</sup>, Zsuzsa Ferencz<sup>φ</sup>, Gábor Vári<sup>†</sup>, Vladimír Matolin<sup>φ</sup>, András Erdőhelyi<sup>φ</sup>,  
Ákos Kukovecz<sup>†</sup>, Zoltán Kónya<sup>†,ψ</sup>*

<sup>†</sup>Department of Applied and Environmental Chemistry, University of Szeged, H-6720 Szeged, Hungary

<sup>φ</sup>Department of Physical Chemistry and Material Science, University of Szeged, H-6720 Szeged, Hungary

<sup>φ</sup>Surface Physics Group, Charles University in Prague, CZ-180 00 Praha 8 – Libeň, Czech Republic

<sup>ψ</sup>MTA-SZTE Reaction Kinetics and Surface Chemistry Research Group, University of Szeged, H-6720 Szeged, Hungary

**ABSTRACT:** 4.8 nm Pt nanoparticles were anchored onto the surface of mesoporous nickel-oxide supports (NiO). Pt/NiO samples were compared to pristine NiO and Pt/SBA-15 silica catalysts in CO<sub>2</sub> hydrogenation to form carbon-monoxide, methane and ethane at 473-673 K. 1 % Pt/NiO were ~20 times and ~1.5 times more active at 493 K compared to Pt/SBA-15 and NiO catalysts, respectively. However, the Pt-free NiO support has an activity of 120% compared to Pt/NiO catalysts at 673 K. In the case of 1% Pt/SBA-15 catalyst, selectivity towards methane was 13 %, while it was 90% and 98% for NiO and 1% Pt/NiO at 673 K, respectively. Exploration of the results of the reactions was performed by Near Ambient Pressure X-ray Photoelectron Spectroscopy (NAP-XPS) as well as in-situ Diffuse Reflectance

1  
2  
3 Infrared Fourier Transform Spectroscopy (DRIFTS). In the case of pure NiO, we found that  
4 the surface of the support was mainly covered by elemental Ni under reaction condition,  
5 where the Ni/NiO<sub>x</sub> system is responsible for the high activity of Pt-free catalyst. In the case of  
6 Pt/NiO, Pt improves the reduction of NiO<sub>x</sub> towards metallic Ni. In the case of the 1 % Pt/NiO  
7 catalysts, the presence of limited amount of Pt resulted in an optimal quantity of oxidized Pt  
8 fraction at 673 K showing the presence of a Pt/PtO<sub>x</sub>/Ni/NiO<sub>x</sub> mixed phase where the different  
9 interfaces may be responsible for the high activity and selectivity towards methane. In the  
10 case of pure NiO under reaction condition, small amounts of formaldehyde as well as  
11 hydrogen perturbed CO [H<sub>n</sub>CO (n=1,2)] were detected. However, in the case of 1 % Pt/NiO  
12 catalysts, besides the absence of formaldehyde a significant amount of H<sub>n</sub>CO (n=2-3) was  
13 present on the surface responsible for the high activity and methane selectivity.  
14  
15  
16  
17  
18  
19  
20  
21  
22

## 23 INTRODUCTION

24  
25 Carbon-dioxide conversion into fuels is highly relevant today both from the process  
26 improvement and from the environmental points of view<sup>1,2,3</sup>. Heterogeneous catalysis<sup>4</sup>,  
27 electrochemistry<sup>5</sup>, photochemistry<sup>6</sup> or photoelectrochemistry<sup>7,8</sup> etc. are used to find the perfect  
28 solution for carbon dioxide reduction towards sufficient energy forming methods.  
29  
30  
31

32 Noble metal (Rh, Ru, Pt, Pd) or Ni, Fe, Co based catalysts are productive materials for  
33 methanation reactions<sup>9,10</sup> and CuO/ZnO/Al<sub>2</sub>O<sub>3</sub> systems are used for methanol synthesis<sup>11</sup>.  
34 MnO<sub>x</sub>/CoO<sub>x</sub> hybrid catalysts are promising candidates for low pressure high energy fuel  
35 synthesis<sup>4</sup>. Pt supported on Nb<sub>2</sub>O<sub>5</sub> or ZrO<sub>2</sub> is also active in low temperature CO<sub>2</sub>  
36 hydrogenation<sup>12</sup>. Nickel based catalysts are cost efficient and have high efficiency in CO<sub>2</sub>  
37 methanation reactions<sup>9</sup>. Pt/NiO systems are active in C=O bond activation<sup>13</sup>, where the  
38 Pt/NiO interface as well as the oxidation state of the support play a role in the reaction  
39 pathways. Size controlled Pt nanoparticles anchored onto the surface of designed mesoporous  
40 NiO films resulted in a high efficiency photoelectrochemical catalyst<sup>7</sup>.  
41  
42  
43  
44  
45  
46  
47

48 Recent developments in engineering the metal–support interaction in Co<sub>3</sub>O<sub>4</sub>, MnO<sub>2</sub>, and CeO<sub>2</sub>  
49 supported Pt nanoparticle systems have resulted in catalysts with enhanced activity in the CO  
50 oxidation reaction<sup>13</sup>. Another major achievement was the 50% reduction of the CO<sub>2</sub>  
51 methanation activation energy by deliberately exploiting the hydrogen spillover  
52 phenomenon<sup>14</sup>. In-situ investigation methods were used successfully to facilitate the in-depth  
53 understanding of the reactions, reactants, intermediates, and the surface chemistry of the  
54  
55  
56  
57  
58  
59  
60

1  
2  
3 catalysts under reaction conditions<sup>15,16,17</sup>. Based on the knowledge accumulated about the  
4 activity, mechanism, and selectivity of the CO<sub>2</sub> hydrogenation reaction, such advances  
5 correspond to major steps beyond trial-and-error catalyst exploration.  
6  
7

8 Despite the potential advantages of Pt/NiO systems, studies on the rational design of Pt/NiO  
9 catalysts are scarce and somewhat contradictory. The structure of the active catalysts as well  
10 as the mechanism of the reaction and the nature of the surface intermediates are hardly  
11 investigated under reaction conditions in CO<sub>2</sub> hydrogenation. From earlier reports one could  
12 infer that the CO<sub>2</sub> hydrogenation reaction over Pt/NiO catalysts may include nickel-oxide  
13 reduction towards elemental nickel with or without Pt enhancement<sup>18</sup>, carbonate and formate  
14 formation on the surface of the metal or the oxide<sup>19,20</sup>, formation of CO and hydrogen  
15 perturbed CO on the metal surface which can turn into CO as well as low weight hydrocarbon  
16 (e.g. CH<sub>4</sub>) products<sup>21</sup>. The debate on these questions is a hot issue today in the field.  
17  
18  
19  
20  
21  
22

23 We report here on anchoring size controlled Pt nanoparticles with 4.8 nm diameter onto the  
24 surface of a designed 3D mesoporous nickel-oxide support. Pt/NiO, pristine NiO as well as Pt  
25 supported SBA-15 catalysts were tested in CO<sub>2</sub> hydrogenation in the gas phase in a flow  
26 reactor between 493-673 K. The catalysts were monitored with Temperature Programmed  
27 Reduction (TPR) and Near Ambient Pressure X-ray Photoelectron Spectroscopy (NAP-XPS)  
28 as well as in-situ Diffuse Reflectance Infrared Fourier Transform Spectroscopy (DRIFTS)  
29 under reaction conditions. 1% Pt/NiO sample had the highest activity in CO<sub>2</sub> hydrogenation at  
30 693 K, where the main product was CH<sub>4</sub>. Pure mesoporous nickel-oxide support showed  
31 significant activity due to the Ni/NiO interface on the surface.  
32  
33  
34  
35  
36  
37

38 The reducibility of oxide supports in the presence of metal catalysts is crucial for deep  
39 understanding of hydrogenation reactions. The lack of knowledge on nickel-oxide supported  
40 Pt systems also conducted our attention to investigate mesoporous nickel oxide supported Pt  
41 nanoparticles with in-situ techniques under parameters of hydrogenation of CO<sub>2</sub>.  
42  
43  
44

45 We found that under reaction conditions, in the case of Pt/NiO catalyst, there is a complex  
46 interface of Ni/NiO<sub>x</sub>/PtO/Pt where Pt boosts the reduction of NiO to metallic Ni on the top  
47 layers via the assistance of oxygen migration to the surface from the bulk. Furthermore, in the  
48 case of the most active 1 % Pt/NiO catalyst, the surface was highly covered by hydrogen  
49 perturbed CO under reaction condition showing the important role of such intermediates  
50 towards the high CH<sub>4</sub> activity and selectivity. Interestingly, in the case of the pristine NiO and  
51  
52  
53  
54  
55  
56  
57  
58  
59  
60

1  
2  
3 the high Pt content Pt/NiO catalyst, formaldehyde was found on the surface, which was stable  
4 and may decompose towards CO and carbonate.  
5  
6  
7

## 8 **EXPERIMENTAL SECTION**

### 9 **Synthesis of 4.8 nm Pt nanoparticles**

10  
11  
12  
13 Synthesis of 4.8 nm particles is based on a modified version of the polyol-method<sup>22,7</sup>. Briefly,  
14 0.04 g Pt(C<sub>5</sub>H<sub>7</sub>O<sub>2</sub>)<sub>2</sub> and 0.035 g polyvinylpyrrolidone (PVP, MW = 40,000) are solved in 5 ml  
15 ethylene-glycol and ultrasonicated for 30 minutes to obtain a homogenous solution. The  
16 reactor is a three-necked round bottom flask, which is evacuated and purged with atmospheric  
17 pressure argon gas for several cycles to get rid of additional oxygen and water. After three  
18 purging cycles, the flask was immersed in an oil bath heated to 200 °C under vigorous stirring  
19 of the reaction mixture as well as the oil bath. After 10 minutes of reaction, the flask was  
20 cooled down to room temperature. The suspension is precipitated by adding acetone and  
21 centrifuging. The nanoparticles are washed by centrifuging with hexane and redispersing in  
22 ethanol for at least 2-3 cycles, and finally redispersed in ethanol.  
23  
24  
25  
26  
27  
28  
29

### 30 **Synthesis of Mesoporous Nickel Oxide support**

31  
32 For the preparation of mesoporous nickel-oxide support (NiO), hard template replica method  
33 was applied<sup>13</sup>. For the synthesis, KIT-6 silica was used as a hard template. For the synthesis of  
34 KIT-6, 27 g of Pluronic-123 block copolymer and 43.5 ml HCl was dissolved in 980 ml  
35 water. After 30 min, 33.3 ml n-butanol was added to the solution at 35 °C under vigorous  
36 stirring. After 1 h of stirring, 58 g of Tetraethyl orthosilicate (TEOS) was added dropwise to  
37 the solution followed by stirring for 24 h at 35 °C. The solution is stored in a capped plastic  
38 autoclave at 40 °C for another 24 h. Then the solid product was filtered, dried at 90 °C  
39 overnight and calcined at 550 °C for 6 h.  
40  
41  
42  
43  
44

45 NiO was prepared through the hard template method using the as-prepared KIT-6. In a typical  
46 synthesis, 4.65 g Ni(NO<sub>3</sub>)<sub>2</sub>·6 H<sub>2</sub>O was dissolved in 8 ml water at 65 °C and in another flask 4  
47 g KIT-6 was dissolved in 40 ml toluene at 65 °C. They were stirring separately for 30 min,  
48 then the second suspension was transferred into the first with 10 ml of toluene. Vigorous  
49 stirring was applied to the mixture at 65 °C until the total evaporation of toluene. After the  
50 evaporation, the precipitated product was collected and dried at 60 °C overnight, followed by  
51 calcination at 300 °C for 6 h. The silica template was completely removed by several washing  
52  
53  
54  
55  
56  
57  
58  
59  
60

1  
2  
3 steps using 200 ml, 2 M aqueous NaOH solution and distilled H<sub>2</sub>O. The sample was washed  
4 to neutral pH. The filtered product was dried at 50 °C overnight.  
5  
6

### 7 Synthesis of SBA-15 mesoporous silica support

8  
9  
10 SBA-15 mesoporous silica support was synthesized from tetraethyl orthosilicate (TEOS) by a  
11 soft template method. Here, 8 g of pre-melted Pluronic-123, 60 ml distilled water and 240 ml  
12 of 2 M HCl solution were mixed at 40 °C for 2 hours. After the dissolution of P-123, 17 g of  
13 TEOS was added dropwise to the mixture at 40 °C and continuous stirring was applied for 20  
14 hours. Stirring was continued for 36 hours at 60 °C. After the synthesis, the product was  
15 filtered and washed with distilled water. Then, the product was heated to 100 °C with a  
16 heating rate of 2 °C·min<sup>-1</sup> and aged for 5 hours; then the temperature was elevated to 550 °C  
17 with a heating rate of 1 °C·min<sup>-1</sup>. After 4 hours of calcination, the product was ready for  
18 further use.  
19  
20  
21  
22  
23  
24  
25  
26

### 27 Synthesis of Mesoporous NiO and SBA-15 supported Pt catalysts

28  
29 To fabricate supported catalysts, the ethanol suspension of Pt nanoparticles and the different  
30 supports (NiO, SBA-15) were mixed in ethanol and sonicated in an ultrasonic bath (40 kHz,  
31 80 W) for 3 hrs. The supported nanoparticles were collected by centrifugation. The products  
32 were washed with ethanol three times before they were dried at 80 °C overnight.  
33  
34  
35  
36  
37

### 38 Hydrogenation of carbon-dioxide in a continuous flow reactor

39  
40 Before the catalytic experiments either in a continuous-flow reactor or in the ambient pressure  
41 XPS chamber the as received catalysts were oxidized in O<sub>2</sub> atmosphere at 573 K for 30 min to  
42 remove the surface contaminants as well as the PVP capping agent<sup>23,24</sup> and thereafter were  
43 reduced in H<sub>2</sub> at 573 K for 60 min.  
44  
45  
46

47 Catalytic reactions were carried out in a fixed-bed continuous-flow reactor (200 mm long with  
48 8 mm i.d.), which was heated externally. The dead volume of the reactor was filled with  
49 quartz beads. The operating temperature was controlled by a thermocouple placed inside the  
50 oven close to the reactor wall, to assure precise temperature measurement. For catalytic  
51 studies small fragments (about 1 mm) of slightly compressed pellets were used. Typically, the  
52 reactor filling contained 20-150 mg of catalyst. In the reacting gas mixture, the CO<sub>2</sub>:H<sub>2</sub> molar  
53  
54  
55  
56  
57  
58  
59  
60

ratio was 1:4, if not denoted otherwise. The CO<sub>2</sub>:H<sub>2</sub> mixture was fed with the help of mass flow controllers (Aalborg), the total flow rate was 50 ml/min. The reacting gas mixture flow entered and left the reactor through an externally heated tube to avoid condensation. The analysis of the products and reactants was performed with an Agilent 6890 N gas chromatograph using HP-PLOTQ column. The gases were detected simultaneously by thermal conductivity (TCD) and flame ionization (FID) detectors. The CO<sub>2</sub> was transformed by a methanizer to methane, and it was also analyzed by FID.

In a typical measurement, after the pretreatment process, the samples were cooled in flowing H<sub>2</sub> to 473 K and the catalysts were introduced to CO<sub>2</sub>:H<sub>2</sub> mixture with a molar ratio of 1:4 with a total flow rate of 50 ml/min at 473 K and the reactor was heated linearly at a rate of 5 K/min up to 673 K and equilibrated for 120 min. After this method, we started measurements in the case of 1% Pt/SBA-15 and 5 % Pt/SBA-15 at 673 K, 643 K, 623 K, 593 K and then were heated back to 613 K, 653 K, 673 K after waiting for constant activity at each temperature (~1 hr). In the case of NiO, 1% Pt/NiO and 5% Pt/NiO catalysts, we used temperatures of 673 K, 583 K, 568 K, 553 K, 538 K and 523 K. We plotted corresponding Arrhenius-plots in the conversion regime of 0.5-10 %.

### Temperature Programmed Reduction (TPR)

The temperature-programmed reduction (TPR) was carried out in a BELCAT-A apparatus using a reactor (quartz tube with 9 mm outer diameter) that was externally heated. Before the measurements, the catalyst samples were treated in oxygen at 573 K for 30 min. Thereafter, the sample was cooled in flowing Ar to room temperature and equilibrated for 15 min. The oxidized sample was flushed with Ar containing 10% H<sub>2</sub>, the reactor was heated linearly at a rate of 20 K·min<sup>-1</sup> up to 1373 K and the H<sub>2</sub> consumption was detected by a thermal conductivity detector (TCD).

Furthermore, after the catalytic experiments, TPR measurements were performed on the spent catalysts to gain information on the quality and quantity of deposited carbon. After running the reactions of CO<sub>2</sub>:H<sub>2</sub> mixtures at 673 K for 120 min, the reactor was flushed with He at the reaction temperature. The sample was subsequently cooled to ambient temperature, the helium flow was changed to H<sub>2</sub>, and the sample was heated up to 1173 K with a 20 K·min<sup>-1</sup> heating rate. The in situ formed products were analyzed and quantified by gas chromatography.

### Near Ambient Pressure X-ray Photoelectron Spectroscopy (NAP-XPS)

An ultra-high vacuum system equipped with a hemispherical analyzer (PHOIBOS series with 1 DLD detector) and a monochromatic  $AlK_{\alpha}$  ( $h\nu=1486.6$  eV) X-ray radiation source was employed to perform the X-ray photoelectron spectroscopy<sup>25</sup>. The binding energy scale of all XPS spectra was calibrated according to the C 1s reference (284.3 eV, which corresponds to the adventitious carbon). However, only the relative energy position of XPS photoelectron lines in each sample is needed to determine the valence band offset (VBO) and the absolute energy calibration for a sample does not affect the ultimate result. The XPS spectra were analysed by fitting the Shirley-type function, which is commonly used in XP spectra deconvolution<sup>26</sup> and a sum of Voigt functions to the experimental results, using the KoI XPD software<sup>24</sup>. The catalysts were pre-treated (oxidized and reduced) before the experiments the same way as before the catalytic measurements. The partial pressure of the oxygen under the oxidation was 20 mbar and in the case of reduction the hydrogen was set to 5 mbar. Under reaction conditions, the ratio of the  $CO_2:H_2$  was set to 1:4 with a total pressure of 5 mbar.

### In-situ Diffuse Reflectance Infrared Fourier Transform Spectroscopy (DRIFTS)

Infrared spectroscopy measurements were carried out with an 'Agilent Cary-670' FTIR spectrometer equipped with 'Harrick Praying Mantis' diffuse reflectance attachment. The sample holder had two  $BaF_2$  windows in the infrared path. The spectrometer was purged with dry nitrogen. The spectrum of the pretreated catalyst was used as background. At room temperature, a  $CO_2$ -to- $H_2$  molar ratio of 1:4 was introduced into the DRIFTS cell. The tubes were externally heated to avoid condensation. The catalyst was heated under the reaction feed linearly from room temperature to 773 K, with a heating rate of  $20\text{ K}\cdot\text{min}^{-1}$  and IR spectra were measured at 50 K intervals. All spectra were recorded between 4000 and  $900\text{ cm}^{-1}$  at a resolution of  $2\text{ cm}^{-1}$ . Typically, 32 scans were registered. Due to the short optical path within the DRIFTS cell, the contribution of the reactant gases was negligibly small, and from gas phase products only the most intense features were observable.

### High Resolution Transmission Electron Microscopy (HR-TEM)

Imaging of the different silica supports, Pt nanoparticles and derived catalysts, as well as the size distribution of the nanoparticles before and after the catalytic reaction, was performed by an FEI TECNAI G2 20 X-Twin high-resolution transmission electron microscope (equipped

1  
2  
3 with electron diffraction) operating at an accelerating voltage of 200 kV. The samples were  
4 drop-cast onto carbon film coated copper grids from ethanol suspension.  
5  
6  
7

### 8 9 Powder X-ray Diffraction (XRD)

10  
11 XRD studies of the silica supports were performed on a Rigaku MiniFlex II instrument with a  
12 Ni-filtered  $\text{CuK}_\alpha$  source in the range of  $2\theta = 10\text{-}80^\circ$ .  
13  
14  
15  
16

### 17 Gas Sorption Measurements

18  
19 The specific surface area (BET method), the pore size distribution and the total pore volume  
20 were determined by the BJH method using a Quantachrome NOVA 2200 gas sorption  
21 analyzer by  $\text{N}_2$  gas adsorption/desorption at  $-196^\circ\text{C}$ . Before the measurements, the samples  
22 were pre-treated in vacuum ( $< \sim 0.1$  mbar) at 473 K for 2 hours.  
23  
24  
25  
26  
27  
28

## 29 **3. RESULTS AND DISCUSSION**

### 30 31 3.1 Characterization of the catalysts

32  
33 Platinum nanoparticles were synthesized by a polyol method from platinum-chloride  
34 precursor using ethylene glycol as a media and PVP as a capping agent<sup>7</sup>. The as-prepared Pt  
35 nanoparticles have a narrow size distribution with an average diameter of  $4.8 \pm 1.5$  nm (Fig.  
36 1/A.). Electron Diffraction patterns confirm the presence of Pt (111), Pt (200), Pt (220) and Pt  
37 (311) crystallite planes characteristic for metallic face-centered cubic (fcc) platinum.  
38  
39

40  
41 Mesoporous nickel oxide was prepared by the replica method using KIT-6 mesoporous silica  
42 as a hard template and SBA-15 silica for reference state support were synthesized by the soft  
43 method using tetraethyl orthosilicate (TEOS) as a template<sup>13</sup>. TEM investigations confirm the  
44 mesoporous structure of the as-prepared mesoporous NiO and SBA-15 supports with a pore  
45 diameter of 3-6 nm (Fig. 1/B., Fig. 1/C.).  
46  
47  
48  
49

50  
51 4.8 nm Pt nanoparticles were successfully loaded onto the surface of the catalyst supports in  
52 both 1 wt% (Fig. 1/C., Fig. 1/D.) as well as in 5 wt% (Fig. 1/E., Fig. 1/F.) concentration. In  
53 case of 1% loading, there is a smooth distribution of the Pt nanoparticles. In the case of 5 %  
54 loading, clusters of 3-7 pieces of Pt nanoparticles were also observed.  
55  
56  
57  
58  
59  
60

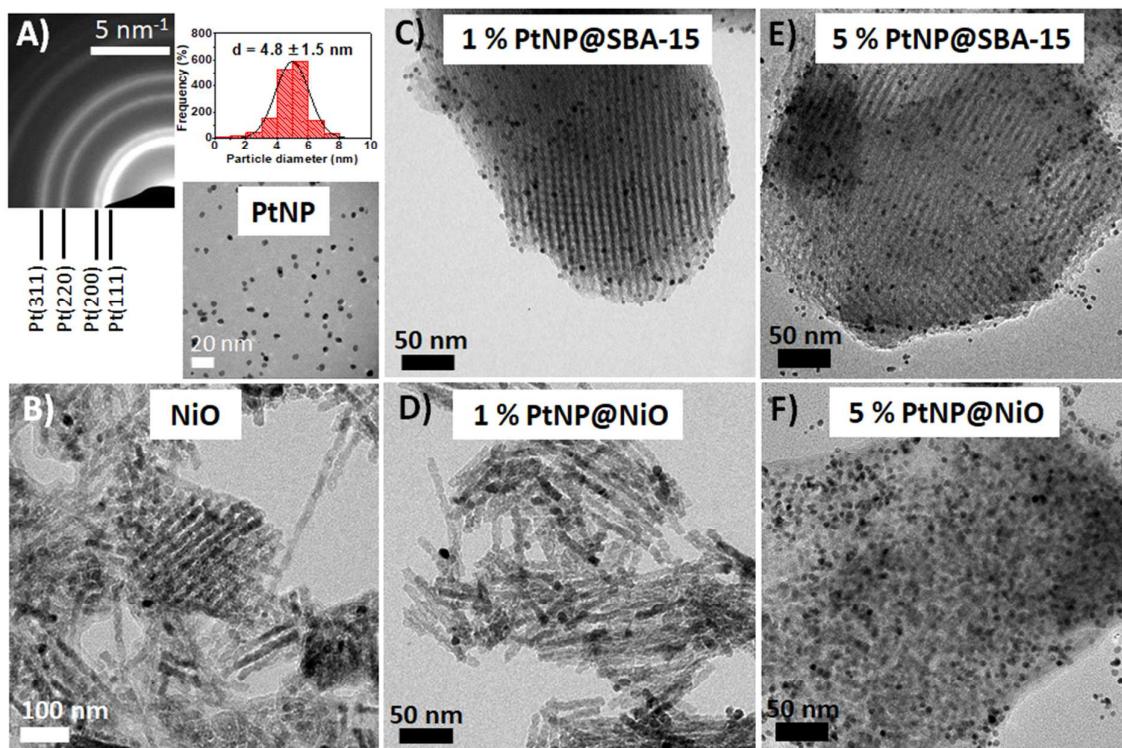


**Figure 1.** Typical TEM images of  $4.8 \pm 1.5$  nm metallic Pt nanoparticles with narrow size distribution (ED pattern shows the presence of metallic Pt) (A), mesoporous nickel-oxide support (B), and 4.8 nm PtNPs supported on SBA-15 and NiO with a loading of 1 wt% (C, D) as well as of 5 wt% (E, F)

The  $N_2$  adsorption/desorption isotherms for pure NiO as well as for SBA-15 silica supports show a type V isotherm characteristic for mesoporous materials (Fig. S1/A., Fig. S1/B.). The type H1 hysteresis loop further strengthening the presence of an ordered structure. The specific surface area was found to be as high as  $127 \text{ m}^2/\text{g}$  and  $820 \text{ m}^2/\text{g}$  for pure NiO and SBA-15, respectively. The XRD patterns of the as-prepared NiO confirms the presence of Ni(II)O (100), (200), (220), (311) and (222) crystal planes, characteristic to the face centered cubic (fcc) nickel(II)- oxide structure (Fig. S1/C.). The broadened diffractions with lower intensity show the amorphous nature of the NiO, which further correlates with the TEM images. In the case of the SBA-15 support, only the weak, broadened diffraction of  $\text{SiO}_2$  (101) was observed indicating the low crystallinity of the silica material (Fig. S1/D.)

### 3.2 Hydrogenation of CO<sub>2</sub> over mesoporous NiO and 4.8 nm Pt nanoparticles supported on SBA-15 and NiO

1% and 5 % 4.8 nm Pt nanoparticles supported on mesoporous nickel oxide as well as pure NiO and 4.8 nm Pt nanoparticle/SBA-15 samples for reference state were tested in CO<sub>2</sub> hydrogenation to form carbon-monoxide, methane, and ethane at 593-673 K in a fix bed flow catalytic reactor. The summarized catalytic results are collected on Fig. 2.

1 % Pt/NiO was ~45 times and ~1.5 times more active at 593 K compared to Pt/SBA-15 and 5 % Pt/NiO catalysts, respectively (Fig. 2/A.). However, the Pt-free NiO support has an activity of ~120% compared to 1 % Pt/NiO catalysts at both 593 K and 673 K (Fig. 2/B.). In the case of 1% Pt/SBA-15 catalyst, selectivity towards methane was 13 %, while it was 90% and 98% for NiO and 1% Pt/NiO at 673 K, respectively (Fig. 2/C., Fig. 2/D.).

In the case of Pt/SiO<sub>2</sub> catalysts, the main product was CO via the water-gas-shift reaction from CO<sub>2</sub> which was formed at the interface of the Pt and SiO<sub>2</sub><sup>27</sup>. In the case of pure NiO, the high selectivity towards CH<sub>4</sub> indicates the formation of metallic nickel on the NiO surface under reaction condition as metallic nickel is a well-known catalyst in CO<sub>2</sub> methanation<sup>9,28</sup>. Pt has no significant conversion enhancing effect on the reactivity of mesoporous nickel-oxide. In the case of the most active 1% Pt/NiO catalyst, 78% conversion was reached at 673K. Size controlled Pt nanoparticles have an activity increasing effect in 1 % loading. However, the activity of 5% Pt/NiO is lower than that of pure NiO catalysts. Also, the excess amount of Pt resulted in enhanced CO production showing the presence of individually working Pt surfaces blocking some of the active NiO sites and Pt/Ni/NiO<sub>x</sub> interphases.

A small amount of ethane was detected in the case of nickel-oxide support. 5% Pt/NiO catalysts produced 3 times more ethane (0.12 %) compared to pure NiO (0.04 %) and 1% Pt/NiO catalyst (0.03 %) (Fig. S2/A.). The catalysts remained stable at 673 K under the reaction condition for at least 2.5 hours (Fig. S2/B.).

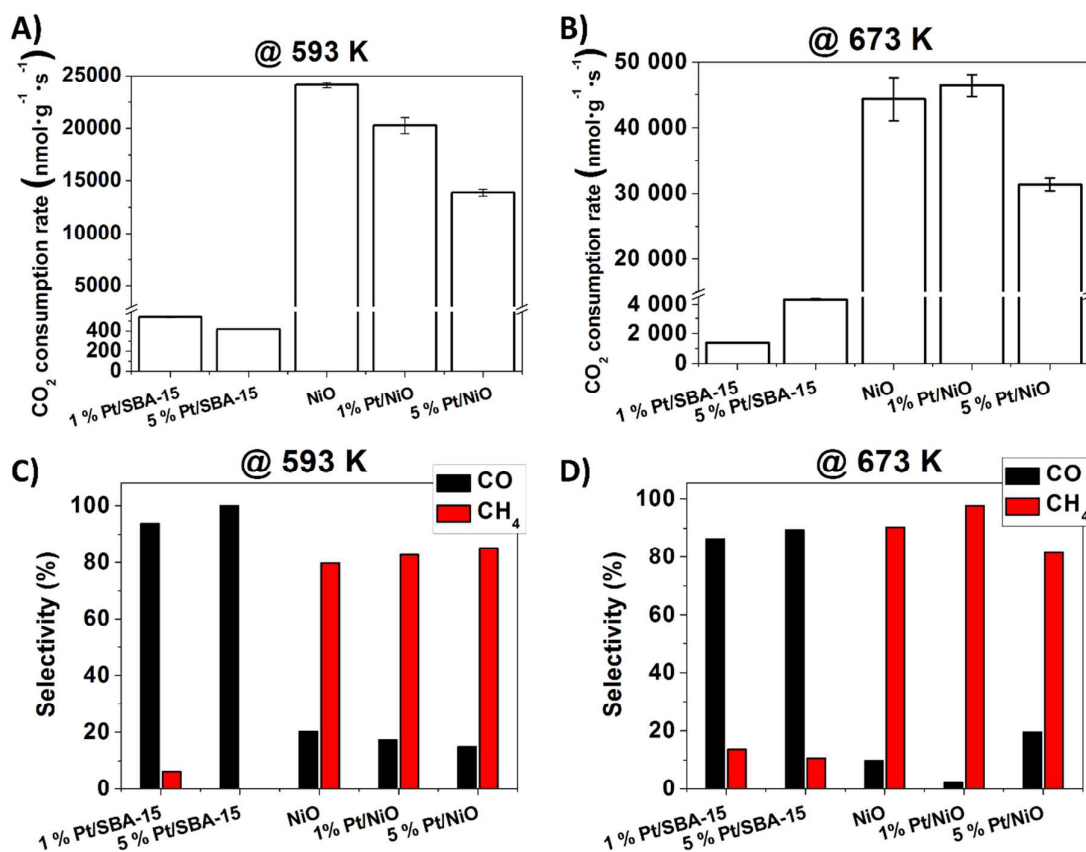


**Figure 2.** CO<sub>2</sub> hydrogenation over 1% and 5% Pt/NiO, Pt/SBA-15 and pure NiO catalysts at 593 K and 673K

Activation energy calculation was determined for all catalysts in the kinetical regime (0.5-10% conversion) at 523-623 K (Fig. S3.). For 1% Pt/SBA-15 and 5 % Pt/SBA-15, the activation energies were 16.7 kcal/mol and 19.4 kcal/mol, respectively. This results are correlated with other studies<sup>10</sup>.

In the case of Pt free mesoporous nickel oxide support, the higher activation energy (25.2 kcal/mol) show the presence of different mechanism. This phenomenon shows different pathway of the reaction as it is clearly seen from the fact that the selectivity towards CH<sub>4</sub> is higher compared to the Pt/SBA-15 systems. These activation energy values for CO as well as for CH<sub>4</sub> formation is comparable for the results from literature<sup>29</sup>.

In the case of mesoporous nickel oxide supported catalyst, the presence of the Pt nanoparticles resulted in a slight decrease of the activation energies. For 1% Pt/NiO and 5 % Pt/NiO, the

1  
2  
3 activation energies were 22.8 kcal/mol and 20.7 kcal/mol, respectively. Pt plays an important  
4 role in the reduction of nickel oxide as well as preferring other reaction routes. For deeper  
5 understanding of Pt/NiO system in this reaction, H<sub>2</sub> TPR, NAP-XPS as well as DRIFTS  
6 studies were performed.  
7  
8  
9

### 10 11 12 3.3 Temperature programmed reduction 13

14 The reduction profile of supported metal catalysts depends on the interaction of the metal with  
15 its support<sup>30</sup>. In present cases the catalysts were oxidized at 573 K for 30 min. In the case of  
16 Pt/SBA-15, there is no significant interaction between Pt and support. The platinum oxide  
17 formed during oxidation treatment can be reduced at 500-850 K. The lower TPR peak is at  
18 580 K, the higher is at 697 K (Fig. S4.). Pt<sup>0</sup> can be obtained in this temperature range on  
19 SBA-15 and SiO<sub>2</sub> according to the literature<sup>31,32</sup>. Where the interaction of Pt with oxide  
20 support is strong as in Pt/NiO case<sup>33</sup>, the positively charged platinum (Pt<sup>2+</sup> or Pt<sup>4+</sup>) is  
21 relatively unstable and is easily reduced to Pt<sup>0</sup>.  
22  
23  
24  
25  
26  
27

28 In the case of the Pt anchored onto mesoporous nickel oxide support, part of the platinum is  
29 reduced at 488 K. However, the reduction of the other part of the platinum take places at  
30 higher temperatures (at the low temperature tailing of the feature of NiO) (Fig. 3.).  
31  
32

33 The reducibility of NiO as catalyst and as catalyst support depends on the morphology,  
34 porosity and the preparation methods. In harmony with the literature<sup>34</sup>, the NiO can be  
35 reduced in two steps (Fig. 3.); the peak at 673 K could be attributed to reduction from Ni<sup>2+</sup> to  
36 Ni<sup>δ+</sup> and the peak at 788 K is the characteristic temperature of the Ni<sup>δ+</sup> to Ni<sup>0</sup> reduction. A  
37 very small TPR peak at 522 K is probably due to the reduction of a trace amount of Ni<sup>3+</sup>.  
38  
39  
40  
41

42 The reducibility of NiO dramatically changes in the presence of Pt. Both characteristic TPR  
43 peaks moved to lower temperature. These changes are increasing with Pt metal content even  
44 at same sizes (4.8nm). In the case of the 1 % Pt/NiO, the TPR peaks are at 668 and 731 K. At  
45 5 % metal content, the peak temperatures moved further to 664 and 713 K (Fig. 3.). In the  
46 case of 5 % Pt content, the H<sub>2</sub> consumption of second peak is less than that of first step,  
47 suggesting that NiO can be reduced to a great degree during the first step. It should be  
48 emphasized that TPR is a dynamic method therefore, if the reduction was carried out under  
49 isothermic condition, the same reduction trend would be achieved at lower temperatures.  
50  
51  
52  
53  
54  
55  
56  
57  
58  
59  
60

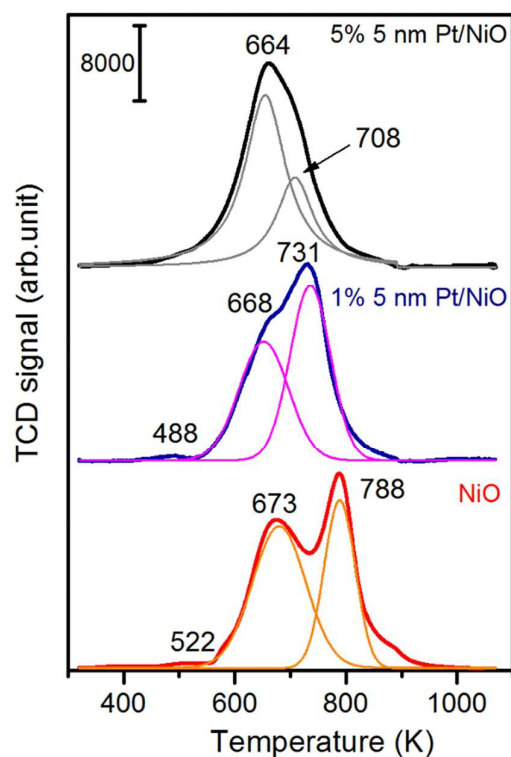


**Figure 3.** TPR profile for NiO and NiO supported 4.8 nm Pt nanoparticles with a loading of 1 % as well as 5 % showing the enhancing effect of Pt on NiO reduction towards metallic nickel.

### 3.4 NAP-X-ray photoelectron spectroscopy during the catalytic reaction

Pure nickel oxide, 5 % Pt/NiO catalyst was tested in NAP-XPS measurements under reaction conditions (573 K – 673 K,  $p = 5$  mbar,  $\text{CO}_2:\text{H}_2$  ratio was 1:4). Before catalytic reactions the catalysts were oxidized in  $\text{O}_2$  at 573 K, and then reduced at 573 K in  $\text{H}_2$  for 30 min. (The XPS spectra recorded during different treatments are presented in the Supporting Information).

In the case of the as-prepared and oxidized NiO, the Ni 2p shows two different Ni states: one corresponds to NiO (853.4 eV) the other is very close to  $\text{Ni}(\text{OH})_2$  form (855.6 eV) (Fig. S5/A.). A strong satellite appeared at 860.6 eV, which is characteristic for NiO. After oxidation a typical Ni  $2p_{3/2}$  structure appeared at 853.1 and 855.1 eV and an intense satellite was detected at 860.4.0 eV. Very similar spectrum was reported previously for polycrystalline and macro-mesoporous NiO<sup>35,36,33</sup>. After reduction at 573 K, the main peak moved to 852.4

eV, and a peak developed at 858.1 eV as a satellite indicated that metallic Ni is dominant<sup>37</sup>, a small but remarkable oxidized fraction remained at 853.2 eV.

The C 1s signals are shown in Fig. S5/B. The as prepared sample contains C 1s features (284.3 and around 288.2 eV) due to the adventitious carbon and precursor molecules. After oxidation-reduction, only a small intensity carbon feature was left at 284.3 eV. Similar spectra were obtained on Pt/NiO for Ni 2p with only differences that after reduction Ni<sup>2+</sup> contribution was not detected. The C 1s due to the template and PVP were removed in oxidation-reduction cycle. The Pt 4f shows mainly Pt<sup>0</sup> chemical state; only a small fraction remained in the partially oxidized state.

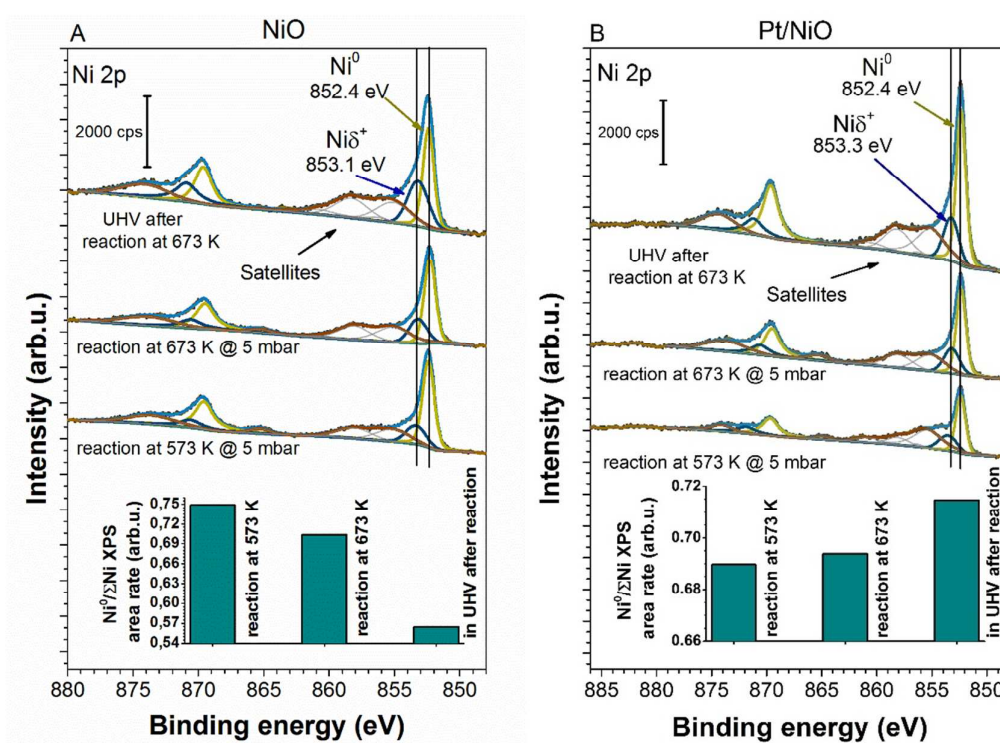


**Figure 4.** Ni 2p XP spectra of NiO (A) and 5 % Pt/NiO (B) under CO<sub>2</sub> hydrogenation conditions and subsequent evacuation at 673 K

Under reaction conditions at 573 K – 673 K, on the surface of NiO the Ni 2p<sub>3/2</sub> appeared at 852.4 eV which corresponds to zero valent Ni<sup>0</sup> (Fig. 4/A.). A shoulder can be detected at 853.1 eV due to Ni<sup>2+</sup> with its satellites at 855.1 and 860.4 eV, which are characteristic for NiO<sup>33,35,36</sup> the latter one appeared only with very small intensity. Two obvious satellites are fitted by peaks with BE near 856.3 eV (hardly detectable) and at 858.1 eV (major) above the

1  
2  
3 main emission of Ni<sup>0</sup> at 852.4 eV which is characteristic for metallic Ni<sup>37</sup>. The satellite for  
4 NiO at 860.4 eV is in well-detectable in the deconvoluted spectrum obtained after vacuum  
5 treatment at 673 K (Fig. 4/A.). In the determination of the ratio of metallic and oxidized  
6 fraction we considered all the six emissions in deconvolution in the Ni 2p<sub>3/2</sub> range.  
7  
8

9  
10 At 5 mbar total pressure and at 573 K, in the case of pure nickel-oxide, the nickel is mainly in  
11 reduced state (74% Ni<sup>0</sup>/ΣNi). The metallic nature of the surface became less significant in  
12 CO<sub>2</sub> hydrogenation at 673 K (~69% Ni<sup>0</sup>/ΣNi) and the following UHV conditions (~ 56 %).  
13 These phenomena may be attributed to the fast migration of the oxygen atoms to the surface  
14 as well as the slow reoxidation of the elemental nickel on the surface by the adsorbed CO<sub>2</sub><sup>38</sup>  
15 or water<sup>39</sup>.  
16  
17  
18  
19

20 Beside Ni 2p, C1s and O1s XP signals were also monitored during reaction conditions at 573  
21 and 673 K (Fig. S6. and Fig.S7.). Intense photoemission peaks developed at 292.7 and 291.3  
22 eV in the case of C1s spectra. These peaks can be attributed to gas phase CO<sub>2</sub> and gas phase  
23 CO formed in the reaction<sup>40</sup>, respectively. These XPS signals disappeared when the surface  
24 was evacuated at 573 or 673 K (Fig. S6.). It is an important observation that a carbon species  
25 remained at 283.2 eV (except adventitious carbon) on the surface after reaction at 573 K.  
26 Very likely this peak corresponds to carbidic carbon<sup>41,42</sup>. The origin of this species is the  
27 result of decomposition of CH<sub>x</sub>. This form markedly decreased on the surface after reaction at  
28 673 K. We suppose in harmony with the literature the carbon on Ni dissolves to the bulk.  
29  
30  
31  
32  
33  
34

35 This was confirmed by TPR spectroscopy when the used catalyst was heated in hydrogen at a  
36 heating rate of 10 K·min<sup>-1</sup>. The amount of the carbon was below the detection (not shown).  
37 Corresponding O 1s signals for gas phase CO and CO<sub>2</sub> were detected at 536.4 and 537.6 eV,  
38 respectively<sup>43</sup> (Fig. S7.). Besides surface (531.0 eV) and lattice (530.0 eV) oxygen XPS  
39 peaks, a relatively broad peak centered at 533 eV was also present. Detailed analysis did not  
40 attempt because the DRIFTS give much precise identification of intermediates and adsorbed  
41 species. This complex peak may contain formate and different carbonates and adsorbed CO  
42 contributions<sup>27,44,8</sup> which were identified by DRIFTS (see below). After evacuation at 673 K,  
43 the intensity of the O 1s region decreased due to desorption (not shown), but it became more  
44 complex as a significant fraction of formate (and formaldehyde) might be transformed to  
45 carbonate as independently detected by DRIFTS (see below). Note that the possibility of  
46 readsorption from background during evacuation cannot be completely excluded.  
47  
48  
49  
50  
51  
52  
53  
54  
55  
56  
57  
58  
59  
60

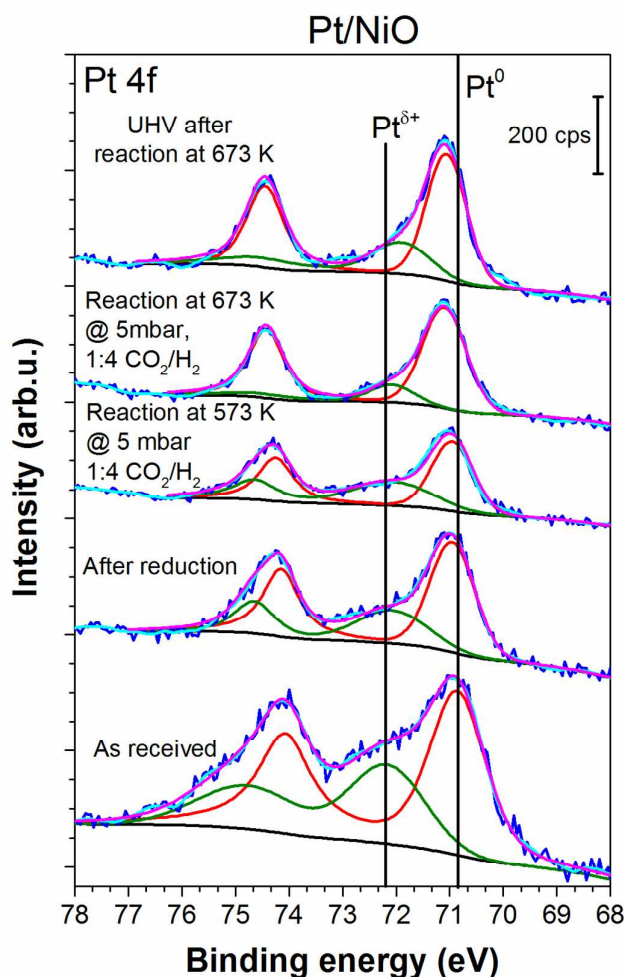


**Figure 5.** Pt 4f XPS spectrum of 5 % Pt/NiO under pretreatment (in O<sub>2</sub> and H<sub>2</sub>) as well as reaction conditions at 5 mbar total pressure of CO<sub>2</sub>:H<sub>2</sub> with a ratio of 1:4 at 573 K and 673 K.

In the case of the 5 % Pt/NiO catalyst, the Ni 2p<sub>3/2</sub> was also followed during reactions at 573 and 673 K and after evacuation at 673 K, respectively (Fig. 4B.). The obtained results are relevant compared to the NAP-XPS studies of the pure NiO catalyst. (In the determination of the ratio of metallic and oxidized fraction we considered all the six emissions of Ni and NiO in deconvolution.) During CO<sub>2</sub> hydrogenation at 573 K, the surface concentration of metallic nickel is 69 % (Fig. 4B.). In the case of the pure nickel-oxide catalyst, at 673 K and after reaction at 673 K, the concentration of the Ni<sup>0</sup> decreased from ~69% to ~56 %. However, in the case of Pt containing catalyst this trend was opposite. This shows a metallic nickel enrichment on the surface after CO<sub>2</sub> hydrogenation at 673 K (~69 %). After reaction at 673 K under UHV condition, the concentration was ~71.5 %. Probably, oxygen diffusion from the

1  
2  
3 bulk also takes place, where the oxygen atoms from the bulk as well as from the surface of the  
4 nickel-oxide support migrate to the Pt nanoparticles helping in the reduction of nickel-oxide.  
5 During reaction at 573 K, a small amount of oxidized Pt was observed (Fig. 5.). Under  
6 reaction conditions at 673 K, the amount of the oxidized fraction decreased. However, when  
7 the catalyst was evacuated at 673 K, the oxidized fraction was regained showing the presence  
8 of the oxygen transferring properties of the Pt nanoparticles from the nickel-oxide to the Pt  
9 catalyst. In addition, we may suppose that the enhanced electron transfer from Pt  
10 nanoparticles to NiO or Ni/NiO interface<sup>40</sup> and oxidation of Pt nanoparticles by CO<sub>2</sub> or CO<sub>2</sub>  
11 derivatives (carbonate-like surface species) also contribute to the increased oxidized Pt  
12 fraction.  
13

14  
15  
16  
17  
18  
19 The other important observation is that the intensity of Ni 2p<sub>3/2</sub> is increasing with the  
20 temperature in the presence of Pt. Besides the reduction of the surface from NiO to elemental  
21 nickel, the bulk 5 % Pt/NiO catalyst showed the presence of a high amount of metallic Ni  
22 observed by separate XRD studies (Fig. S8.). Furthermore, a slight sharpening of the Pt (111)  
23 diffraction peak was observed showing the aggregation of the Pt nanoparticles during the  
24 catalytic reaction resulting in the increase of the Ni 2p<sub>3/2</sub> intensity after reaction. These  
25 phenomena show that Pt assist nickel (Ni + NiO) enrichment on the surface which is crucial  
26 in the activity and selectivity of the catalyst in the hydrogenation of CO<sub>2</sub>.  
27  
28  
29  
30  
31  
32

33 On Pt/NiO catalysts the oxidation states of platinum, Pt 4f<sub>7/2</sub> and Pt 4f<sub>5/2</sub> were also monitored  
34 (Fig. 5.). The as received sample contains Pt<sup>0</sup> and Pt<sup>2+</sup> states in 3:1 ratio. After reduction of  
35 the catalyst at 573 K, the 4f<sub>5/2</sub> appeared at 71.1 eV indicating that the platinum is in metallic  
36 state<sup>45</sup>. After careful analyzing of the spectrum, a small shoulder could be detected at 71.9 eV.  
37 This weak shoulder may indicate that a small fraction is in a partially oxidized state probably  
38 due to the electronic interaction of Pt with Ni/NiO interface<sup>46</sup>. The final state effect arising  
39 from the small particles size<sup>47</sup> probably can be ruled out because the particle sizes of Pt did  
40 not change during the reaction and after vacuum treatment according to our HRTEM  
41 experiments. Carbon XPS signal was hardly detectable after high temperature evacuation.  
42 TPR spectroscopy was able to detect a small amount of methane formation (T<sub>p</sub> = 600 K) when  
43 the used catalyst was heated in hydrogen (not shown).  
44  
45  
46  
47  
48  
49  
50

51 The carbon and oxygen signals during the reaction were identical with that obtained with pure  
52 nickel oxide catalyst. Typical O 1s obtained on Pt/NiO in the reaction is shown in Fig. S7/B.  
53 The freshly reduced Pt surface is very active, so CO adsorption always occurs from the  
54 background in a certain amount. Therefore, we focus to the spectra obtained under reaction  
55  
56  
57  
58  
59  
60

1  
2  
3 conditions (573 and 673 K). It is remarkable that when increasing the reaction temperature,  
4 the intensities of lattice oxygen (530.1 eV) and surface oxygen (531.1 eV) slightly decreased  
5 due to the further reduction of NiO. Peaks at 537.6 and 536.4 eV corresponds to gas phase  
6 CO<sub>2</sub> and CO, respectively<sup>43</sup>. A broad peak between 531 and 535 eV may compose C=O  
7 bonded species (probably formaldehyde), adsorbed CO and adsorbed formate and carbonate  
8 intermediates (which were identified by DRITS; see below). After evacuation at 673 K, the  
9 intensities of gas phase components (CO and CO<sub>2</sub>) drastically decreased. The intensities of  
10 other components decreased only slightly (not shown).  
11  
12  
13  
14  
15  
16  
17

### 18 3.5 Infrared spectra during CO<sub>2</sub> hydrogenation at elevated temperatures

19  
20 For catalytic reactions, the exploration of surface species formed during the catalytic  
21 processes plays a decisive role in the understanding of the reaction mechanism. Towards this  
22 goal, DRIFT spectra were monitored at increasing reaction temperatures, in the presence of  
23 the reactant mixture/products. In all cases the different catalysts were pretreated in oxygen at  
24 573 K followed by reduction in H<sub>2</sub> at 573 K. The assignment of IR bands and the detailed  
25 description is based on the vibrational fingerprints of relevant surface species, which were  
26 reported in previous publications. The IR bands observed during the present work and their  
27 origins are collected in Table 1. Note that the denoted wave numbers may vary by  $\pm 5 \text{ cm}^{-1}$   
28 within one data set as a function of temperature.  
29  
30  
31  
32  
33  
34  
35

36 When the reaction mixture was introduced to the Pt-free SBA-15, no adsorption forms were  
37 detected at any temperatures. The DRIFT spectra for 5% 5nm Pt/SBA-15 in the CO<sub>2</sub>:H<sub>2</sub>  
38 mixture are shown in Fig. S9. The band at 2072 cm<sup>-1</sup> started to develop already at 300 K.  
39 From 373 K, the intensity increased and it was present even at high temperature (723 K). This  
40 peak is attributed to the formation of adsorbed CO which forms during the catalytic reaction.  
41 This kind of CO bonds to the Pt particles in linear form<sup>48,49</sup>. This peak was also detected  
42 when the Pt content was 1% in the case of the Pt/SBA-15 catalysts (not shown). In that case  
43 the peak corresponding to the linear CO appeared first at 423 K with lower intensity. No other  
44 absorption band for adsorbed CO was detected. The linearly adsorbed CO form appeared  
45 when CO was introduced to this surface at 300 K, too.  
46  
47  
48  
49  
50  
51  
52  
53  
54  
55  
56  
57  
58  
59  
60

**Table 1.** Characteristic frequencies ( $\pm 5 \text{ cm}^{-1}$ ) for surface intermediates formed in the  $\text{CO}_2 + \text{H}_2$  reaction on pure NiO, Pt/NiO and Pt/SBA-15 catalysts

Intermediates	Vibration mode	NiO	1% Pt/NiO	5% Pt/NiO	Pt/SBA-15	Ref.
bidentate carbonate $\text{CO}_3^-$	$\nu_3(\text{O-C-O})_a$ $\nu_3(\text{O-C-O})_s$	1302 1383 1538 1620	1305 1576	1305 1530		50,51
bicarbonate $\text{HCO}_3^-$	$\nu_2(\text{O-C-O})_a$ $\nu_3(\text{O-C-O})_s$ $\delta(\text{COH})$	1648 1375 1214	1630 1378 1214	1626 1376 1214		51
carbon monoxide CO	linear bridge		2052 1912 (weak)	2061 1918	2078 1940	48,49, 52
carbonyl hydrides $\text{H}_n\text{CO}$ (n=1,2)		1880 (weak)	1840 (strong)	1840 (weak)	1817	21,53, 19,54
formaldehyde $\text{H}_2\text{CO}$	$\nu\text{CO}$ $\nu\text{CH}$	1770 (weak)	-	1770 (strong) 2840		55,56, 57,58
formate $\text{HCOO}^-$	$\nu_a(\text{OCO})$ $\nu_s(\text{OCO})$ $\gamma(\text{OCO})$ $\nu\text{CH}$	1576 1340  2837	1572 1376	1576 1350 1379 2838	2840	59,60, 61,57

The evaluation of the low wavenumber region of Pt/SBA-15 is particularly difficult, since the silica-like sample itself has very strong absorptions at  $\sim 1940$ ,  $\sim 1820$ - $1570$  and  $\sim 1200$ - $1000 \text{ cm}^{-1}$ <sup>52</sup>. Although these features should be accounted for by the background spectrum, they might also change as a function of temperature and thus disturb our spectra. We tentatively assign the features observed to this effect. We cannot exclude that a small absorption bands at  $1942$  and  $1825 \text{ cm}^{-1}$  reflect the appearance of bridge bonded  $\text{CO}$ <sup>62</sup>. The latter could be influenced by adsorbed hydrogen. This feature was also detected on  $\text{Rh/SiO}_2$ <sup>21</sup>. The low-frequency shift in the presence of hydrogen has been attributed to the formation of Rh carbonyl hydrides<sup>53,63,54</sup>. It is assumed that the CO in this complex could easily dissociate. It is important to mention that C-H stretching was not observed (Fig. S9.). These phenomena correlate with the catalytic tests, where the SBA-15 supported Pt nanoparticles produced

mainly CO and almost no other products. At the Pt/SiO<sub>2</sub> interfaces, the reverse-water-shift gas (RWSG) reaction resulted in the formation of CO from CO<sub>2</sub><sup>27</sup>.

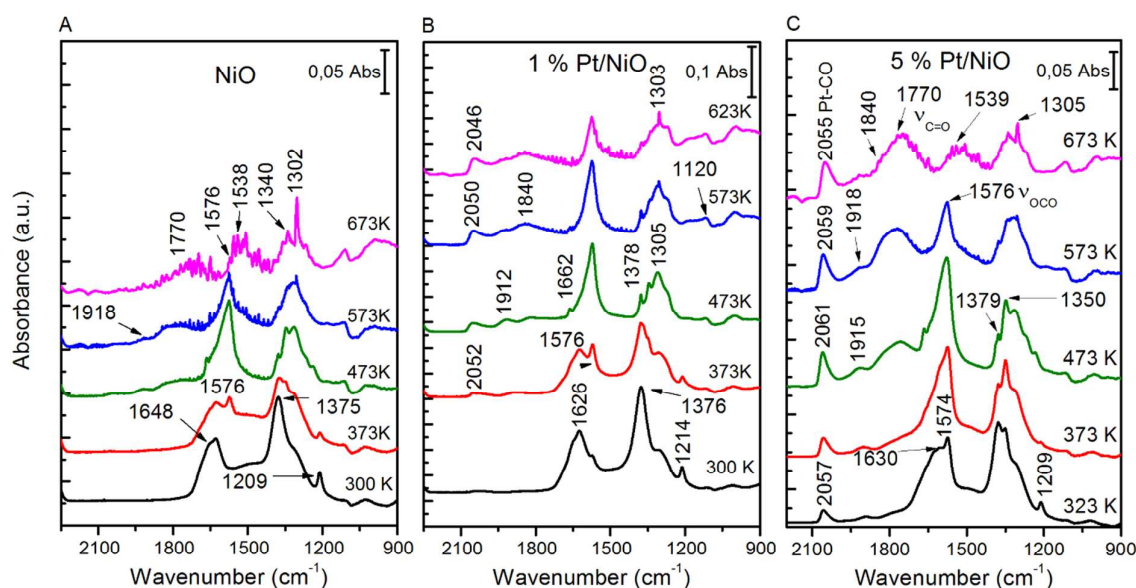
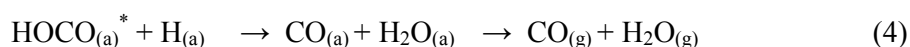
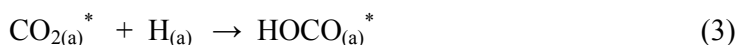


**Figure 6.** DRIFT spectra obtained during linear heating (20 K·min<sup>-1</sup>) in CO<sub>2</sub>:H<sub>2</sub> mixture (1:4) on NiO (A), 1% Pt/NiO (B) and 5% Pt/NiO (C) catalysts (average Pt particle size is 4.8 nm).

When CO<sub>2</sub>:H<sub>2</sub> mixture was introduced to the pretreated NiO catalyst, a broad band appeared at 1648 cm<sup>-1</sup> and two narrow ones at 1375 and 1209 cm<sup>-1</sup> at 300 K, as represented in Fig. 6/A. These bands correspond to the bicarbonate (HCO<sub>3</sub><sup>-</sup>) species and can be assigned to ν<sub>2</sub>(OCO)<sub>a</sub>, ν<sub>3</sub>(OCO)<sub>s</sub> and δ<sub>4</sub>(COH), respectively<sup>51</sup>. The adsorption of CO<sub>2</sub> on NiO gives two adsorption bands in the IR spectrum at 1620 and 1383 cm<sup>-1</sup> (not shown), which are assigned to carbonate ion on the oxide<sup>50</sup>. Carbonate structures may be formed via coordination of a bent CO<sub>2</sub><sup>δ-</sup> towards an oxygen atom<sup>64</sup>.

When the sample was heated to 473 K, two peaks developed at 1576 and 1340 cm<sup>-1</sup>. These bands can be assigned to the formation of formate species. These species were observed on

Rh/MgO catalyst during CO<sub>2</sub>:H<sub>2</sub> adsorption<sup>19</sup>, and after adsorption of HCOOH on TiO<sub>2</sub> powder<sup>59,60</sup> and TiO<sub>2</sub> (110)<sup>61</sup> due to asymmetric and symmetric stretch of (OCO). The corresponding  $\nu(\text{CH})$  vibration is detected at 2837 cm<sup>-1</sup> from 473 K (Fig. S9/A.). Around 473 K a weak band appeared at 1875-1900 cm<sup>-1</sup> probably due hydrogen perturbed CO.

When the sample was further heated (573-673 K), the intensity of C-H stretching vibrational features decreased. Two peaks remained or developed at 1576 and 1302 cm<sup>-1</sup>, very probably due to asymmetric and symmetric bidentate carbonates ( $\nu_3(\text{OCO})_a$  and  $\nu_3(\text{OCO})_s$ ). A broad, weak peak at around 1770 cm<sup>-1</sup> is detectable as C=O containing species (H<sub>2</sub>CO). Also a weak absorption band is detectable at 1918 cm<sup>-1</sup> due to hydrogen perturbed CO, which is located on metallic Ni. From 573 K a sharp peak for gas phase CH<sub>4</sub> was detected indicating that the reaction between CO<sub>2</sub> and H<sub>2</sub> is occurring (Fig. S10/A.).

When 4.8 nm Pt nanoparticles were anchored onto NiO at different content, new spectral features were observed. The bicarbonate-formate-bidentate carbonate surface reaction sequence remained in the 300-623 K temperature range. In the case of the 1% Pt/NiO catalyst, peaks at 1576, 1378 cm<sup>-1</sup> may represent the formate in  $\nu_{\text{assym}}(\text{OCO})$  and  $\nu_s(\text{OCO})$  modes, respectively<sup>65</sup> (Fig. 6/B.). As new feature, linearly adsorbed CO at 2046-2061 cm<sup>-1</sup> appeared already at room temperature. Small intensity bridge bonded CO showed up at 1915-1918 and 1840 cm<sup>-1</sup>. The latter species is presumably CO perturbed by adsorbed hydrogen.

It is clear that the Pt adatom catalyzes the transformation of bicarbonate to formate; peak at ~1630 cm<sup>-1</sup> (bicarbonate) is hardly detectable at 373 K in the case of 5% Pt/NiO sample (Fig. 6/C.). The corresponding  $\nu(\text{CH})$  vibration at 2837-40 cm<sup>-1</sup> is detectable already at 323-373 K (Fig. S/10.). The detection of a strong CO signal indicates that the Pt is an active center for the dissociation of CO<sub>2</sub> in the presence of hydrogen. Without hydrogen the formation of adsorbed CO was not observed. The appearance of gas phase CH<sub>4</sub> in FTIR spectra above 473 K demonstrates that a catalytic reaction occurs between CO<sub>2</sub> and hydrogen. The bands for adsorbed CO and CH and for gas phase methane (Fig. S10/B., S10/C.) appeared at higher temperature at low (1%) Pt content. Independently from the Pt content, an IR band was observed at 1840 cm<sup>-1</sup>, which was probably due to CO perturbed by hydrogen: so-called carbonyl hydrides<sup>21,54</sup>. BOC-MP calculations have also shown that the dissociation of H<sub>n</sub>CO, where n=1,2 or 3 is energetically more favorable than the direct dissociation of CO on Pd and Pt<sup>66</sup>. Although there is significant evidence to support the idea that C-O bond cleavage is hydrogen assisted, no direct evidence for the existence of H<sub>n</sub>CO surface species during the hydrogenation of CO or CO<sub>2</sub> has been reported. Williams et al.<sup>67</sup> have proposed a mechanism

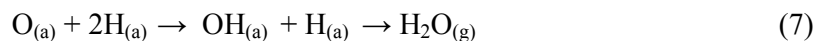
1  
2  
3 for CO<sub>2</sub> hydrogenation to methane over Rh based on the observations reported above in which  
4 H<sub>2</sub>CO<sub>(a)</sub>-like species is involved. Its decomposition leads to CH<sub>2(a)</sub> which either forms carbon  
5 or is hydrogenated to CH<sub>4</sub>.  
6

7  
8 A significantly strong absorption feature at 1770 cm<sup>-1</sup> is detected at 5% Pt content (Fig. 6/C.).  
9 This band corresponds to the C=O double bond, thus it can be assigned to formaldehyde  
10 (vCO). This peak was observed in gas phase formaldehyde<sup>68</sup>, after adsorption of  
11 formaldehyde on NiO<sup>55</sup>, on TiO<sub>2</sub>-supported Rh<sup>56</sup> and Pt and Au catalysts<sup>57</sup>. It is evident that  
12 the formation of formyl/formaldehyde species is catalyzed by Pt particles in CO<sub>2</sub>:H<sub>2</sub> reaction,  
13 because it was difficult to detect on clean NiO. As this intermediate is still present even at  
14 high temperature (673 K), we may suppose that its formation rate is higher than its  
15 decomposition rate. Very probably the formyl (H<sub>2</sub>CO) species could decompose to the final  
16 products. Mainly at 5% Pt content, we have two important IR peaks, that can both be assigned  
17 to hydrogen. It is perturbed CO: one is H<sub>2</sub>CO<sub>(a)</sub>- like species or carbonyl hydrides at 1840  
18 cm<sup>-1</sup>, the other is of formyl/formaldehyde, at 1770 cm<sup>-1</sup> which contains C=O double bond.  
19 Both of them could be important in the CO<sub>2</sub>:H<sub>2</sub> reaction. It is clear that the carbonyl hydrides  
20 are more reactive. vCH<sub>2</sub> was detected even at 323-373 K indicating that in this case (compare  
21 to the Pt-free case) some hydrocarbon fragment, very probably formate is formed (Fig.  
22 S10/B., S10/C.). Gas phase methane appeared already from 523 K. The H<sub>2</sub>CO<sub>(a)</sub> is rather  
23 stable, its contribution to the gas phase products is less than the hydrogen perturbed CO.  
24  
25  
26  
27  
28  
29  
30  
31  
32  
33  
34

35 The question arises: what is the source of the formation of formyl/formaldehyde detected on  
36 Pt/NiO? Recently it was found that formaldehyde forms in the interaction of HCOOH with Pt  
37 supported TiO<sub>2</sub><sup>58</sup>. In this interaction it was supposed that both vacancies and Pt sites catalyze  
38 formaldehyde formation. It is important that the formate is produced on pure NiO, and the  
39 hydrogen is dissociating on Pt nanoparticles. We may assume that hydrogen atoms migrate to  
40 the metal-support interface and react with formate there to form formyl/formaldehyde. As  
41 adsorbed formyl was not detectable at low Pt content, we suppose that large amount of atomic  
42 hydrogen is necessary for this reaction. Though the dissociation of hydrogen takes place at  
43 300 K, formyl forms from 423 K at 5% Pt content, indicating that the hydrogen spillover from  
44 the metal to NiO or its reaction with formate is an activated process. This type of formyl  
45 could then decompose to CO at higher temperatures<sup>57</sup>.  
46  
47  
48  
49  
50  
51  
52

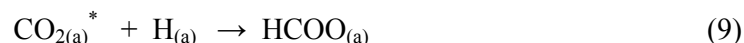
53 Taking into account the product distribution in the CO<sub>2</sub>:H<sub>2</sub> reaction and the observed  
54 intermediates on NiO and Pt/NiO catalysts we may assume that the reversed water gas shift  
55 mechanism (RWGS) to form CO is also valid in a certain extent (steps 1-4). The methane  
56  
57  
58  
59  
60

1  
2  
3 formation can be deduced through formation of surface  $H_nCO$  ( $n= 1,2,3$ ) which was offered  
4 on supported  $Pt^{21}$  and  $Rh^{18}$  catalysts:

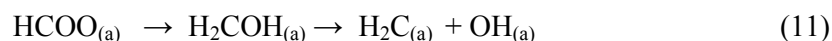


9  
10  
11  
12  
13  
14  
15  
16  
17  
18 The reaction steps 5-8 could be dominant at 1% Pt content. The  $CH_n$  species may recombine a  
19 small extent to form ethane.

20  
21  
22 On Pt-free NiO, the formate pathways come to the front as formate is the main surface  
23 intermediate observed in DRIFTS:



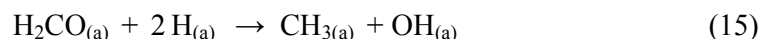
26  
27  
28  
29  
30 The formate intermediate may produce methane, too<sup>19</sup>:



33  
34  
35  
36  
37 When the Pt content is high, the formate may convert to formaldehyde as was observed in our  
38 DRIFTS experiments and published on Pt/SiO<sub>2</sub> and Pt/TiO<sub>2</sub><sup>21,44</sup>:



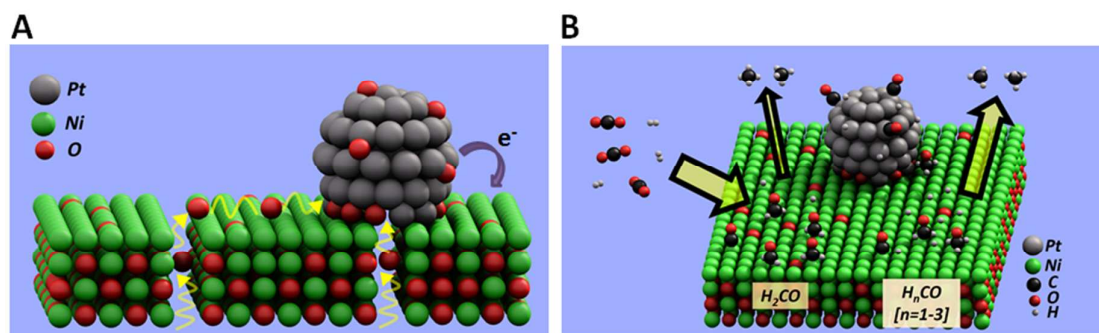
40  
41  
42  
43 The formaldehyde may decompose to  $CO^{44}$  at high temperature but may forms  $CH_4^{21}$ , too<sup>69</sup>:



47  
48  
49  
50  
51  
52  
53  
54 In summary, from the XPS measurements we may conclude that the  $CO_2$  hydrogenation at  
55 573 K and 673 K takes place on the surface and interface of a complex  $NiO_x/Ni/PtO_x/Pt$   
56  
57

1  
2  
3 catalyst. Pt boosts oxygen migration to the surface as well as changes the reaction mechanism  
4 and activity, resulting in a high performance CH<sub>4</sub> producing catalyst with 1% 4.8 nm Pt  
5 nanoparticles on the surface of the mesoporous nickel oxide support (Fig. 7A).  
6  
7

8  
9 In the case of pure nickel-oxide during CO<sub>2</sub> hydrogenation over 673 K, small amounts of  
10 formaldehyde and hydrogen perturbed CO are present at the surface to form mostly methane  
11 observed by DRIFTS studies. In the case of the most active and methane selective 1% Pt/NiO  
12 sample, formaldehyde species are absent but a significant amount of hydrogen perturbed CO  
13 is present. The number of perturbing hydrogen atoms are even higher (2-3) compared to pure  
14 NiO catalyst (1-2). These results show, that the presence of Pt helps to produce the high  
15 numbered hydrogen perturbed CO complex, which in turn is producing methane in the CO<sub>2</sub>  
16 hydrogenation reaction. The formation of formaldehyde does not help methane formation  
17 process (Fig. 7/B.).  
18  
19  
20  
21  
22  
23  
24  
25



37  
38 **Figure 7.** (A) Schematic view of a presence of complex NiO<sub>x</sub>/Ni/PtO<sub>x</sub>/Pt catalyst, where Pt  
39 boosts oxygen migration to the surface; (B) Schematic view of the proposed mechanism of  
40 CO<sub>2</sub> hydrogenation over hydrogen perturbed CO, where Pt flood the surface with hydrogen  
41 to enhance the CH<sub>4</sub> formation.  
42  
43  
44  
45  
46

## 47 CONCLUSION

48  
49 Here in this project, size controlled Pt nanoparticles with 4.8 nm diameter were anchored onto  
50 the surface of 3D mesoporous nickel-oxide support. Pt/NiO, pristine NiO as well as Pt  
51 supported on SBA-15 catalysts were tested in CO<sub>2</sub> hydrogenation reaction in the gas phase in  
52 a flow reactor at 473 – 673 K as well as investigated with Temperature Programmed  
53 Reduction (TPR). The catalysts were also monitored under reaction conditions with Near  
54  
55  
56  
57  
58  
59  
60

1  
2  
3 Ambient Pressure X-ray Photoelectron Spectroscopy (NAP-XPS) as well as in-situ Diffuse  
4 Reflectance Infrared Fourier Transform Spectroscopy (DRIFTS).

5  
6 1 % Pt/NiO was ~20 times and ~1.5 times more active at 493 K compared to Pt/SBA-15 and  
7 NiO catalysts, respectively. However, the Pt-free NiO support has an activity of 120%  
8 compared to Pt/NiO catalysts at 673 K. In the case of 1% Pt/SBA-15 catalyst, selectivity  
9 towards methane was 13 %, while it was 90% and 98% for NiO and 1% Pt/NiO at 673 K,  
10 respectively.  
11  
12  
13  
14

15 In the case of pure NiO, we found that the surface of the support was mainly covered by  
16 elemental Ni under reaction conditions, where the Ni/NiO<sub>x</sub> system is responsible for the high  
17 activity of Pt-free catalyst. In the case of Pt/NiO, Pt improves the reduction of NiO<sub>x</sub> towards  
18 metallic Ni. We found oxidized Pt at 673 K with XPS at 5% Pt content showing the presence  
19 of a Pt/PtO<sub>x</sub>/Ni/NiO<sub>x</sub> mixed phase, where the different interfaces may be responsible for the  
20 high activity and selectivity towards methane.  
21  
22  
23  
24

25 In the case of pure NiO under reaction condition, formaldehyde as well as a small amount  
26 hydrogen perturbed CO was detected. However, in the case of 1 % Pt/NiO, significant  
27 amounts of H<sub>n</sub>CO species were presented on the surface showing that the reaction towards  
28 methane goes through the dissociation of H<sub>n</sub>CO on the surface. The formyl/formaldehyde  
29 form could be a rather inactive intermediate due to its high thermal stability.  
30  
31  
32  
33  
34  
35

### 36 **ACKNOWLEDGEMENT**

37  
38  
39 This paper was supported by the János Bolyai Research Scholarship of the Hungarian  
40 Academy of Sciences as well as the Hungarian Research Development and Innovation Office  
41 through grants NKFIH OTKA PD 120877 of AS. ÁK, GH and KZ are grateful for the fund of  
42 NKFIH (OTKA) K112531 & NN110676, PD 115769 and K120115, respectively. This  
43 collaborative research was partially supported by the “Széchenyi 2020” program in the  
44 framework of GINOP-2.3.2-15-2016-00013 “Intelligent materials based on functional  
45 surfaces – from syntheses to applications” project. NAP-XPS measurements were governed in  
46 in Prague, Charles University under the program of Ceric-Eric Consortium.  
47  
48  
49  
50  
51  
52  
53  
54  
55  
56  
57  
58  
59  
60

## ASSOCIATED CONTENT

### Supporting Information.

Detailed experimental procedures and supplementary figures and table. This material is available free of charge via the Internet at <http://pubs.acs.org>.

## AUTHOR INFORMATION

### Corresponding Author

\* [sapia@chem.u-szeged.hu](mailto:sapia@chem.u-szeged.hu)

### Author Contributions

‡These authors contributed equally.

## REFERENCES

- (1) Chiang, J. H.; Hopper, J. R. Kinetics of the Hydrogenation of Carbon Dioxide over Supported Nickel. *Ind. Eng. Chem. Prod. Res. Dev.* **1983**, *22*, 225–228.
- (2) Vannice, M. A. The Catalytic Synthesis of Hydrocarbons from H<sub>2</sub>/CO Mixtures over the Group VIII Metals II. The Kinetics of the Methanation Reaction over Supported Metals. *J. Catal.* **1975**, *37* (3), 462–473.
- (3) Schlutter, M.; Götz, M.; Lefebvre, J.; Prabhakaran, P.; Schneider, J.; Rönsch, S.; Matthischke, S.; Bajorh, S. Review on Methanation – From Fundamentals to Current Projects. *Fuel* **2015**, *166*, 276–296.
- (4) Li, C.-S.; Melaet, G.; Ralston, W. T.; An, K.; Brooks, C.; Ye, Y.; Liu, Y.-S.; Zhu, J.; Guo, J.; Alayoglu, S.; et al. High-Performance Hybrid Oxide Catalyst of Manganese and Cobalt for Low-Pressure Methanol Synthesis. *Nat. Commun.* **2015**, *6*, 6538.
- (5) Giesbrecht, P. K.; Herbert, D. E. Electrochemical Reduction of Carbon Dioxide to Methanol in the Presence of Benzannulated Dihydropyridine Additives  
Electrochemical Reduction of Carbon Dioxide to Methanol in the Presence of Benzannulated Dihydropyridine Additives. *ACS Energy Lett.* **2017**.
- (6) Boston, D. J.; Xu, C.; Armstrong, D. W.; Macdonnell, F. M. Photochemical Reduction of Carbon Dioxide to Methanol and Formate in a Homogeneous System with

- 1  
2  
3 Pyridinium Catalysts. *J. Am. Chem. Soc.* **2013**, *135*, 16252–16255.  
4  
5 (7) Sapi, A.; Varga, A.; Samu, G. F.; Dobo, D. G.; Juhasz, K. L.; Takacs, B.; Varga, E.;  
6 Kukovecz, A.; Konya, Z.; Janaky, C. Photoelectrochemistry by Design: Tailoring the  
7 Nanoscale Structure of Pt/NiO Composites Leads to Enhanced Photoelectrochemical  
8 Hydrogen Evolution Performance. *J. Phys. Chem. C* **2017**, *121*, 12148–12158.  
9  
10 (8) Halasi, G.; Gazsi, A.; Bansagi, T.; Solymosi, F. Applied Catalysis A : General  
11 Catalytic and Photocatalytic Reactions of H<sub>2</sub> + CO<sub>2</sub> on Supported Au Catalysts.  
12 "Applied Catal. A, Gen. **2015**, *506*, 85–90.  
13  
14 (9) Frontera, P.; Macario, A.; Ferraro, M.; Antonucci, P. Supported Catalysts for CO<sub>2</sub>  
15 Methanation: A Review. *Catalysts* **2017**, *7* (2), 59.  
16  
17 (10) F. Solymosi, A. E. Hydrogenation of CO<sub>2</sub> to CH<sub>4</sub> over Alumina-Supported Noble  
18 Metals. *J. Mol. Catal. A Chem.* **1980**, No. 8, 471.  
19  
20 (11) Jadhav, S. G.; Vaidya, P. D.; Bhanage, B. M.; Joshi, J. B. Catalytic Carbon Dioxide  
21 Hydrogenation to Methanol: A Review of Recent Studies. *Chem. Eng. Res. Des.* **2014**,  
22 *92*, 2557–2567.  
23  
24 (12) Takashi, I.; Tokio, I. Hydrogenation of Carbon Dioxide and Carbon Monoxide over  
25 Supported Platinum Catalysts. *J. Chem. Soc. Faraday Transit.* **1986**, *82*, 1681–1686.  
26  
27 (13) An, K.; Alayoglu, S.; Musselwhite, N.; Plamthottam, S.; Melaet, G.; Lindeman, A. E.;  
28 Somorjai, G. A. Enhanced CO Oxidation Rates at the Interface of Mesoporous Oxides  
29 and Pt Nanoparticles. *J. Am. Chem. Soc.* **2013**, *135* (44), 16689–16696.  
30  
31 (14) Patil, U. V.; Ramgir, N. S.; Karmakar, N.; Bhogale, A.; Debnath, A. K.; Aswal, D. K.;  
32 Gupta, S. K.; Kothari, D. C. CO<sub>2</sub> Hydrogenation Studies on Co and CoPt Bimetallic  
33 Nanoparticles under Reaction Conditions Using TEM, XPS and NEXAFS. *Nano Lett.*  
34 **2014**, *136* (May), 4792–4796.  
35  
36 (15) Zheng, F.; Alayoglu, S.; Guo, J.; Pushkarev, V.; Li, Y.; Glans, P.; Chen, J.; Somorjai,  
37 G. In-Situ X-Ray Absorption Study of Evolution of Oxidation States and Structure of  
38 Cobalt in Co and CoPt Bimetallic Nanoparticles (4 Nm) under Reducing (H<sub>2</sub>) and  
39 Oxidizing (O<sub>2</sub>) Environments. *Nano Lett.* **2011**, *11*, 847–853.  
40  
41 (16) Sapi, A.; Thompson, C.; Wang, H.; Michalak, W. D.; Ralston, W. T.; Alayoglu, S.;  
42 Somorjai, G. A. Recovery of Pt Surfaces for Ethylene Hydrogenation-Based Active  
43  
44  
45  
46  
47  
48  
49  
50  
51  
52  
53  
54  
55  
56  
57  
58  
59  
60

- 1  
2  
3 Site Determination. *Catal. Letters* **2014**, *144* (7), 1151–1158.
- 4  
5 (17) Alayoglu, S.; Krier, J. M.; Michalak, W. D.; Zhu, Z.; Gross, E.; Somorjai, G. A. In Situ  
6 Surface and Reaction Probe Studies with Model Nanoparticle Catalysts. *ACS Catal.*  
7 **2012**, *2*, 2250–2258.
- 8  
9  
10 (18) Khachatur, M.; Manukyan, V.; Avetisyan, A. g.; Shuck, C.; Chatilyan, H. A.;  
11 Rouvimov, S.; Kharatyan, S. L.; Mukasyan, A. S. Nickel Oxide Reduction by  
12 Hydrogen: Kinetics and Structural Transformations. *J. Phys. Chem. C* **2015**, *119* (28),  
13 16131–16138.
- 14  
15  
16 (19) Erdohelyi, A., Solymosi F., B. T. Infrared Study of the Surface Interaction between H<sub>2</sub>  
17 and CO<sub>2</sub> over Rhodium on Various Supports. *J. Chem. Soc. Farad. Trans.* **1981**, *77*,  
18 2645–2657.
- 19  
20  
21  
22 (20) M. Tóth, J. Kiss, A. Oszkó, G. Pótári, B. L.; Erdöhelyi, A. Hydrogenation of Carbon  
23 Dioxide on Rh, Au and Au–Rh Bimetallic Clusters Supported on Titanate Nanotubes,  
24 Nanowires and TiO<sub>2</sub>. *Top. Catal.* **2012**, *55*, 747–756.
- 25  
26  
27 (21) Fisher, I. A.; Bell, A. T. A Comparative Study of CO and CO<sub>2</sub> Hydrogenation over  
28 Rh/SiO<sub>2</sub>. *J. Catal.* **1996**, *162* (259), 54–65.
- 29  
30  
31 (22) Gómez-Pérez, J.; Dobó, D. G.; Juhász, K. L.; Sápi, A.; Haspel, H.; Kukovecz, Á.;  
32 Kónya, Z. Photoelectrical Response of Mesoporous Nickel Oxide Decorated with Size  
33 Controlled Platinum Nanoparticles under Argon and Oxygen Gas. *Catal. Today* **2016**,  
34 1–7.
- 35  
36  
37 (23) Borodko, Y.; Habas, S. E.; Koebel, M.; Yang, P.; Frei, H.; Somorjai, G. A. Probing the  
38 Interaction of Poly(vinylpyrrolidone) with Platinum Nanocrystals by UV - Raman and  
39 FTIR. *J. Phys. Chem. B* **2006**, *110*, 23052–23059.
- 40  
41  
42 (24) Borodko, Y.; Humphrey, S. M.; Tilley, T. D.; Frei, H.; Somorjai, G. A. Charge-  
43 Transfer Interaction of Poly(vinylpyrrolidone) with Platinum and Rhodium  
44 Nanoparticles. *J. Phys. Chem. C* **2007**, No. 111, 6288–6295.
- 45  
46  
47 (25) Luo, I.; Monai, M.; Wang, C.; Lee, J. D.; Duchoň, T.; Dvořák, F.; Matolín, V.; Murray,  
48 C. B.; Fornasiero, P.; Gorte, R. J. Unraveling the Surface State and Composition of  
49 Highly Selective Nanocrystalline Ni–Cu Alloy Catalysts for Hydrodeoxygenation of  
50 HMF. *Catal. Sci. Technol.* **2017**, *8*, 1735–1743.
- 51  
52  
53  
54  
55  
56  
57  
58  
59  
60

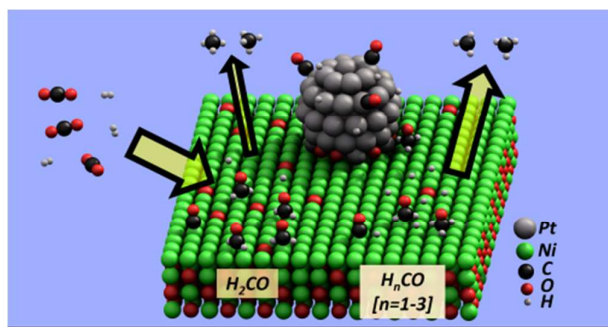
- 1  
2  
3 (26) Shirley, D. A. High-Resolution X-Ray Photoemission Spectrum of the Valence Bands  
4 of Gold. *Phys. Rev. B* **1972**, *5*, 4709.  
5  
6  
7 (27) Kattela, S.; Yana, B.; Chena, J. G.; Li, P. CO<sub>2</sub> Hydrogenation on Pt, Pt/SiO<sub>2</sub> and  
8 Pt/TiO<sub>2</sub>: Importance of Synergy between Pt and Oxide Support. *J. Catal.* **2016**, *343*,  
9 115–126.  
10  
11  
12 (28) Delmelle, R.; Duarte, R. B.; Franken, T.; Burnat, D.; Holzer, L.; Borgschulte, A.; Heel,  
13 A. Development of Improved Nickel Catalysts for Sorption Enhanced CO<sub>2</sub>  
14 Methanation. *Int. J. Hydrogen Energy* **2016**, *41* (44), 20185.  
15  
16  
17 (29) Wang, X.; Shi, H.; Szanyi, J. Controlling Selectivities in CO<sub>2</sub> Reduction through  
18 Mechanistic Understanding. *Nat. Commun.* **2017**, *8* (1), 513.  
19  
20  
21 (30) Anderson, J. R. *Structure of Metallic Catalysts*; Academic Press, 1975.  
22  
23  
24 (31) Liu, Q.; Joshi, U. A.; Kevin, U.; Regalbuto, J. R. The Control of Pt and Ru  
25 Nanoparticle Size on High Surface Area Supports. *Phys. Chem. Chem. Phys.* **2014**, No.  
26 16, 26431–26435.  
27  
28  
29 (32) Goguet, A.; Schweich, D.; Candy, J. Preparation of a Pt/SiO<sub>2</sub> Catalyst II . Temperature-  
30 Programmed Decomposition of the Adsorbed Platinum Tetrammine Hydroxide  
31 Complex under Flowing Hydrogen, Oxygen, and Argon. *J. Catal.* **2003**, *220*, 280–290.  
32  
33  
34 (33) Nie, L.; Yu, J.; Li, X.; Cheng, B.; Liu, G.; Jaroniec, M. Enhanced Performance of  
35 NaOH-Modified Pt/TiO<sub>2</sub> toward Room Temperature Selective Oxidation of  
36 Formaldehyde. *Environ. Sci. Technol.* **2013**, *47*, 277–2783.  
37  
38  
39  
40 (34) Shan, W.; Luo, M.; Ying, P.; Shen, W.; Li, C. Reduction Property and Catalytic  
41 Activity of Ce<sub>(1-x)</sub>Ni<sub>x</sub>O<sub>2</sub> Mixed Oxide Catalysts for CH<sub>4</sub> Oxidation. *Appl. Catal. A*  
42 *Gen.* **2003**, *246*, 1–9.  
43  
44  
45 (35) Roberts, M. W.; Smart, S. T. C. The Defect Structure of Nickel Oxide Surfaces as  
46 Revealed by Photoelectron Spectroscopy. *J. Chem. Soc. Farad. Trans.* **1984**, No. 80,  
47 2957–2968.  
48  
49  
50  
51 (36) Grosvenor, A. P.; Biesinger, M. C.; Smart, R. S. C.; McIntyre, N. S. New  
52 Interpretations of XPS Spectra of Nickel Metal and Oxides. *Surf. Sci.* **2006**, *600*, 1771–  
53 1779.  
54  
55  
56  
57  
58  
59  
60

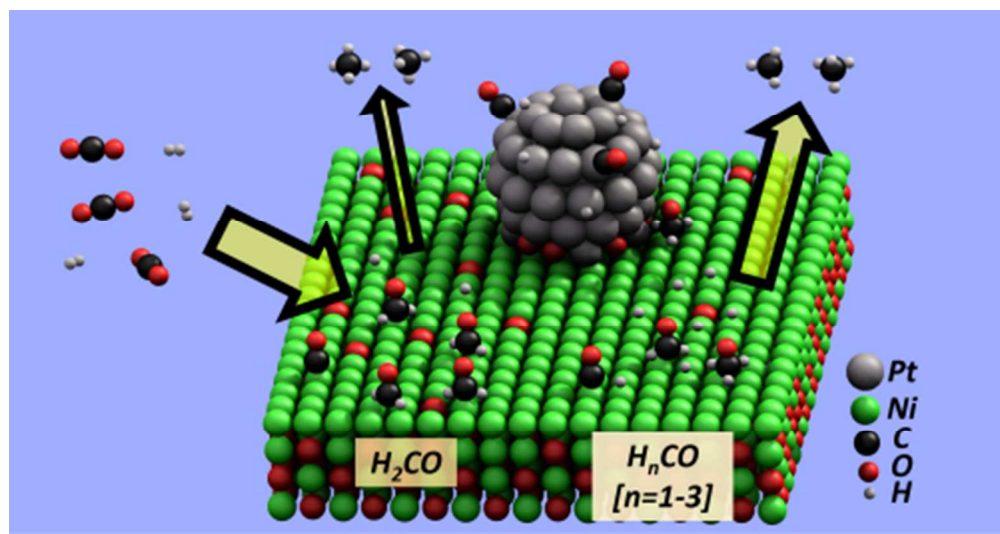
- 1  
2  
3 (37) Kucharczyk, B.; Tylus, W.; Okal, J.; Chęćmanowski, J.; Szczygieł, B. The Pt-NiO  
4 Catalysts over the Metallic Monolithic Support for Oxidation of Carbon Monoxide and  
5 Hexane. *Chem. Eng. J.* **2016**, *309*, 288–297.  
6  
7  
8 (38) Antill, J. E., Wartburton, E. J. Oxidation of Nickel by Carbon Dioxide. *J. Electrochem.*  
9 *Soc.* **1967**, *114*, 1215–1221.  
10  
11  
12 (39) Kelemen, S. R. The Reaction of Carbon and Water as Catalyzed by a Nickel Surface.  
13 *Appl. Surf. Sci.* **1987**, *28* (4), 439–474.  
14  
15  
16 (40) Commerce, U.S.S. of. NIST X-ray Photoelectron Spectroscopy Database  
17 <https://www.srdata.nist.gov/xps/>.  
18  
19  
20 (41) Wiltner, A.; Linsmeier, C. Formation of Endothermic Carbides on Iron and Nickel.  
21 *Phys. Status Solidi Appl. Res.* **2004**, *201* (5), 881–887.  
22  
23  
24 (42) Steinbach, F.; Kiss, J.; Krall, R. Identification and Stability of CH<sub>3</sub>, CH<sub>2</sub> and CH  
25 Species on Co and Ni Surfaces, A PES Investigation. *Surf. Sci.* **1985**, *157*, 401–412.  
26  
27  
28 (43) Calderón, S. K.; Grabau, M.; Óvári, L.; Kress, B.; Steinrück, H. P.; Papp, C. CO  
29 Oxidation on Pt(111) at near Ambient Pressures. *J. Chem. Phys.* **2016**, *144*, 044706.  
30  
31  
32 (44) Lesiak, B.; Stobinski, L.; Malolepszy, A.; Mazurkiewicz, M.; Kövér, L.; Tóth, J.  
33 Journal of Electron Spectroscopy and Preparation of Graphene Oxide and  
34 Characterisation Using Electron Spectroscopy. *J. Electron Spectros. Relat. Phenomena*  
35 **2014**, *193*, 92–99.  
36  
37  
38 (45) Commerce, U. S. S. of. NIST X-ray Photoelectron Spectroscopy Database.  
39  
40  
41 (46) Vayssilov, G. N.; Lykhach, Y.; Migani, A.; Staudt, T.; Petrova, G. P.; Tsud, N.; Skála,  
42 T.; Bruix, A.; Illas, F.; Prince, K. C.; et al. Support Nanostructure Boosts Oxygen  
43 Transfer to Catalytically Active Platinum Nanoparticles. *Nat. Commun.* **2011**, *10*, 310–  
44 315.  
45  
46  
47  
48 (47) Henry, C. R.; Luminy, C. De; Cedex, M. Surface Studies of Supported Model  
49 Catalysts. *Surf. Sci. Rep.* **1998**, *31*, 231–325.  
50  
51  
52 (48) Raskó, J. CO-Induced Surface Structural Changes of Pt on Oxide-Supported Pt  
53 Catalysts Studied by DRIFTS. *J. Catal.* **2003**, *217*, 478–486.  
54  
55  
56 (49) S. Ishi, Y. Ohno, B. V. An Overview on the Electronic and Vibrational Properties Of  
57  
58  
59  
60

- 1  
2  
3 Adsorbed CO. *Surf. Sci.* **1985**, *161*, 349–372.
- 4  
5 (50) Bennett, C., Ueno, A.; Hochmuth, J. K. Interaction of CO<sub>2</sub>, CO, and NiO Studied by  
6 Infrared Spectroscopy. *J. Catal.* **1977**, *235*, 225–235.
- 7  
8  
9 (51) Baltrusaitis, J.; Schuttlefield, J.; Zeitler, E.; Grassian, V. H. Carbon Dioxide  
10 Adsorption on Oxide Nanoparticle Surfaces. *Chem. Eng. J.* **2011**, *170* (2–3), 471–481.
- 11  
12 (52) Ferencz, Z.; Erdo, A.; Baan, K.; Oszko, A.; Óvári, L.; Kónya, Z.; Papp, C.; Steinrück,  
13 H.-P.; Kiss, J. Effects of Support and Rh Additive on Co-Based Catalysts in the  
14 Ethanol Steam Reforming Reaction. *ACS Catal.* **2014**, *4*, 1205–1218.
- 15  
16  
17 (53) Henderson, M. A.; Worley, S. D. An Infrared Study of the Hydrogenation of Carbon  
18 Dioxide on Supported Rhodium Catalysts. *J. Phys. Chem.* **1985**, *20* (1982), 1417–1423.
- 19  
20  
21 (54) Solymosi, F.; Knözinger, H. Infrared Spectroscopic Study of the Adsorption and  
22 Reactions of CO<sub>2</sub> on K-Modified Rh/SiO<sub>2</sub>. *J. Catal.* **2015**, *177* (1990), 166–177.
- 23  
24  
25 (55) Truong, C. M.; Wu, M.; Goodman, D. W. Adsorption of Formaldehyde on Nickel  
26 Oxide Studied by Thermal Programmed Desorption and High-Resolution Electron  
27 Energy Loss Spectroscopy. *J. Am. Chem. Soc.* **1993**, *67* (13), 3647–3653.
- 28  
29  
30 (56) Raskó, J.; Kecskés, T.; Kiss, J. Formaldehyde Formation in the Interaction of HCOOH  
31 with Pt Supported on TiO<sub>2</sub>. *J. Catal.* **2004**, *224*, 261–268.
- 32  
33  
34 (57) Raskó, J.; Kecskés, T.; Kiss, J. Adsorption and Reaction of Formaldehyde on TiO<sub>2</sub>-  
35 Supported Rh Catalysts Studied by FTIR and Mass Spectrometry. *J. Catal.* **2004**, *226*,  
36 183–191.
- 37  
38  
39 (58) Kecskés, T.; Raskó, J.; Kiss, J. FTIR and Mass Spectrometric Studies on the  
40 Interaction of Formaldehyde with TiO<sub>2</sub> Supported Pt and Au Catalysts. *Appl. Catal. A*  
41 *Gen.* **2004**, *273*, 55–62.
- 42  
43  
44 (59) Chuang, C.; Wu, W.; Huang, M.; Huang, I.; Lin, J. FTIR Study of Adsorption and  
45 Reactions of Methyl Formate on Powdered TiO<sub>2</sub>. *J. Catal.* **1999**, *434*, 423–434.
- 46  
47  
48 (60) Liao, L.; Wu, W.; Chen, C.; Lin, J. Photooxidation of Formic Acid vs Formate and  
49 Ethanol vs Ethoxy on TiO<sub>2</sub> and Effect of Adsorbed Water on the Rates of Formate and  
50 Formic Acid Photooxidation. *J. Phys. Chem. B* **2001**, *105*, 7678–7685.
- 51  
52  
53 (61) Chang, Z.; Thornton, G. Effect of Pd on the Interaction of Formic Acid with TiO<sub>2</sub>(110).
- 54  
55  
56  
57  
58  
59  
60

- 1  
2  
3 *Surf. Sci.* **2000**, *459*, 303–309.  
4
- 5 (62) Brieger, C.; Melke, J.; Kaghazchi, P.; Roth, C. CO Adsorption on Platinum  
6 Nanoparticles - the Importance of Size Distribution Studied with In-Situ DRIFTS and  
7 DFT Calculations C. Brieger. *ECS Trans.* **2015**, *69* (17), 249–253.  
8  
9
- 10 (63) Solymosi, F.; Erdőhelyi, A.; Kocsis, M. Surface Interaction between H<sub>2</sub> and CO on  
11 Rh/Al<sub>2</sub>O<sub>3</sub>, Studied Adsorption and Infrared Spectroscopic Measurements. *J. Catal.*  
12 **1980**, *436*, 428–436.  
13  
14
- 15 (64) Freund, H.; Robert, M. W. Surface Chemistry of Carbon Dioxide. *Surf. Sci. Rep.* **1996**,  
16 *25*, 225–273.  
17  
18
- 19 (65) Ishi, S. I.; Ohno, Y.; Viswanathan, B. An Overview on the Electronic and Vibration  
20 Properties of CO. *Surf. Sci.* **1985**, *161*, 349–372.  
21  
22
- 23 (66) Bell, T.; Shustorovich, E. Analysis of CO Hydrogenation Pathways Using the Bond-  
24 Order- Conservation Method. *J. Catal.* **1988**, *113*, 341–352.  
25  
26
- 27 (67) Williams, K. J.; Boffa, A. B.; Salmeron, M.; T., B. A.; Somorjai, G. A. The Kinetics of  
28 CO<sub>2</sub> Hydrogenation on Rh Foil Promoted by Titania Overlayers. *Catal. Letters* **1991**, *9*,  
29 415–426.  
30  
31
- 32 (68) Brown, L. R.; Hunt, R. H.; Pine, A. S. Wavenumbers , Line Strengths , and  
33 Assignments in the Doppler-Limited Spectrum of Formaldehyde from 2700 to 3000  
34 Cm<sup>-1</sup>. *J. Mol. Spectrosc.* **1979**, *75*, 406–428.  
35  
36  
37
- 38 (69) Wang, X.; Shi, H.; Kwak, J. H.; Szanyi, J. Mechanism of CO<sub>2</sub> Hydrogenation on  
39 Pd/Al<sub>2</sub>O<sub>3</sub> Catalysts : Kinetics and Transient DRIFTS-MS Studies. *ACS Catal.* **2015**, *5*,  
40 6337–6349.  
41  
42  
43  
44  
45  
46  
47  
48  
49  
50  
51  
52  
53  
54  
55  
56  
57  
58  
59  
60

## TOC Graphics





TOC Graphic

85x44mm (150 x 150 DPI)